Research Article | Vol. 31, No. 15 / 17 Jul 2023 / Optics Express 24821
Optics EXPRESS

49 W carrier-envelope-phase-stable few-cycle 2.1 µm OPCPA at 10 kHz

MAXIMILIAN F. SEEGER,[1,2] DOMINIK KAMMERER,[1] JOHANNES BLÖCHL,[1,2] MARCEL NEUHAUS,[1,2] VLADIMIR PERVAK,[1] THOMAS NUBBEMEYER,[1,2,*] AND MATTHIAS F. KLING[1,2,3,4]

[1]Ludwig-Maximilians-Universität, Munich, 85748 Garching, Germany
[2]Max Planck Institute of Quantum Optics, 85748 Garching, Germany
[3]SLAC National Accelerator Laboratory, Menlo Park, CA 94025, USA
[4]Applied Physics, Stanford University, Stanford, CA 94305, USA
[*]thomas.nubbemeyer@physik.uni-muenchen.de

Abstract: We demonstrate a mid-infrared optical parametric chirped pulse amplifier (OPCPA), delivering 2.1 µm center wavelength pulses with 20 fs duration and 4.9 mJ energy at 10 kHz repetition rate. This self-seeded system is based on a kW-class Yb:YAG thin-disk amplifier driving a CEP stable short-wavelength-infrared (SWIR) generation and three consecutive OPCPA stages. Our SWIR source achieves an average power of 49 W, while still maintaining excellent phase and average power stability with sub-100 mrad carrier-envelope-phase-noise and 0.8% average power fluctuations. These parameters enable the OPCPA setup to drive attosecond pump probe spectroscopy experiments with photon energies in the water window.

1. Introduction

Ultrafast spectroscopy with extreme ultraviolet (XUV) and soft X-ray pulses has become an important tool for studying electron dynamics in atoms [1], solids [2,3], nanostructures [4] and biomolecules [2,5]. Especially near-edge absorption spectroscopy at the K- and L-edges of various atoms with photon energies in the so-called water window ranging from the carbon K-edge at ~280 eV to the oxygen K-edge at ~530 eV has drawn a lot of research interest lately [6–8]. Large synchrotron or X-ray free-electron laser (XFEL) facilities are capable of generating soft X-ray pulses with high flux but are typically limited to pulse durations in the 10-100 fs range [9,10], therefore lacking the temporal resolution to resolve the fundamental electron dynamics happening on below-femtosecond timescales [11]. More recently, several techniques have been developed for the generation of isolated attosecond pulses from XFEL-sources. However, as these sources rely on self-amplified spontaneous emission, they suffer from a large timing jitter on the order of femtoseconds and an unstable temporal pulse shape, making single-shot measurements necessary [12,13].

The development of broadband sources based on high harmonic generation (HHG) has led to a revolution in the field of XUV and soft X-ray spectroscopy as it has enabled the generation of coherent XUV and soft X-ray attosecond pulses [14,15] from a compact tabletop source.

For a long time, titanium doped sapphire (Ti:Sapphire) based laser driven HHG systems have been the back bone of ultrafast XUV spectroscopy. However, Ti:Sapphire systems suffer from the limited average power output due to the large quantum defect of the active material [16] and parasitic amplified spontaneous emission [17]. Additionally, extending the photon energy cutoff of the generated harmonics into the soft X-ray regime is not easily achievable with Ti:Sapphire lasers due to its rather short wavelength emission at 800 nm. The HHG photon cutoff energy scales with the ponderomotive energy $U_p \propto I_L \lambda_L^2$ [18–20], where I_L is the intensity and λ_L is the wavelength of the driving light field. While increasing the HHG cutoff energy by enhancing the laser intensity is possible, the achievable results are limited by ionization effects in the HHG

#493326 https://doi.org/10.1364/OE.493326
Journal © 2023 Received 18 Apr 2023; revised 9 Jun 2023; accepted 13 Jun 2023; published 12 Jul 2023

Optics EXPRESS

gas target and the associated loss of phase matching [20]. Further increase of the HHG cutoff energies thus requires driving lasers with longer wavelengths.

Ultrashort pulses in the 2–6 µm region can be generated in systems based on II-VI semiconductors such as chromium doped zinc selenide (Cr:ZnSe) and chromium doped zinc sulfide (Cr:ZnS) lasers. These systems have proved to be capable of delivering multi-mJ pulses at kHz repetition rate [21], > 100 W average power in cw operation [22] and pulse duration in the few-cycle regime [23], making them promising candidates for future HHG driving sources extending the photon cutoff even beyond the oxygen K-edge. However, combining high average power and pulse energies with few-cycle durations has not yet been achieved, thus, II-VI semiconductor lasers are not yet used for driving soft-X-ray beamlines.

These limitations have led to the development of high-power short wavelength infrared (SWIR) and mid-infrared (MIR) OPCPA setups, driven by ytterbium doped yttrium-aluminum-garnet (Yb:YAG) laser systems, as pump sources for HHG beamlines. Yb:YAG sources can achieve kW-scale power levels using regenerative thin-disk (TD) amplifier [24], Innoslab [25], or large mode area fiber [26] approaches. Nevertheless, all of them suffer from the limited gain bandwidth of the material, preventing direct few-cycle pulse generation and typically limiting the pulse duration to hundreds of femtoseconds [27], which makes them unsuitable for direct generation of high harmonics. However, Yb:YAG based sources have proven to be excellent pump sources for optical parametric chirped pulse amplification setups. The combination of the broadband amplification achievable at a center wavelength of 2.1 µm in degenerate optical parametric amplification (OPA) and the high pump power attainable from Yb:YAG lasers enables few-cycle pulse generation with multi-mJ pulse energies [28] or >100W of output power for longer pulses [29]. Figure 1 shows an overview of state-of-the-art high energy SWIR- and MIR-OPCPA systems.

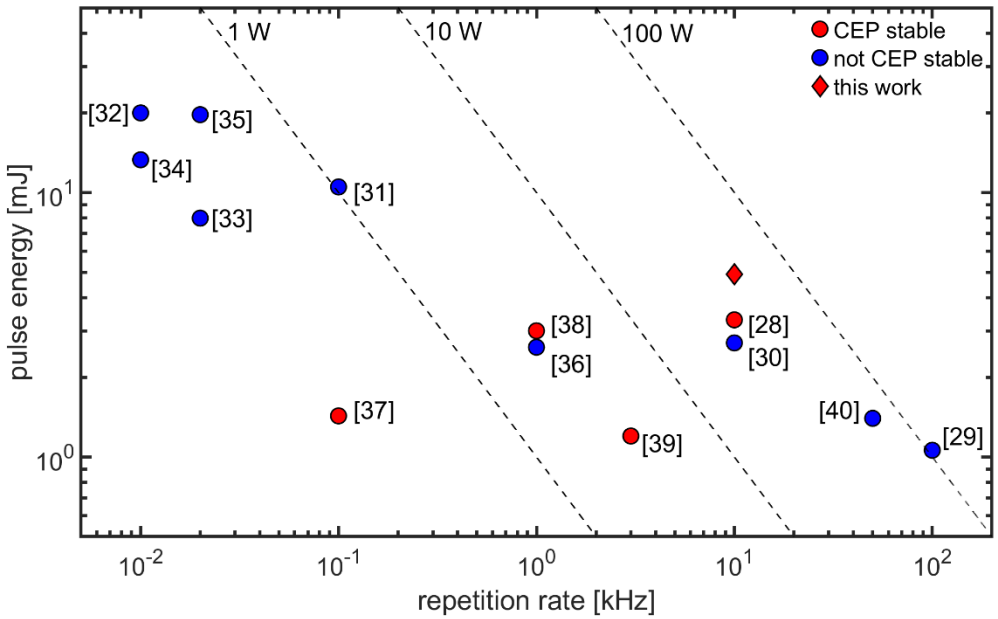

Fig. 1. Overview of high pulse energy SWIR and MIR OPCPA setups. CEP stable systems are displayed in red [28,37–39]. Sources without CEP stability are shown in blue [29–36,40]. The dashed lines mark lines of constant average power.

Optics EXPRESS

Therefore, these setups are exceptionally well suited to drive attosecond experiments relying on the generation of XUV and soft-X-ray attosecond pulses with photon energies in the water window region [41].

In this article, we demonstrate a high pulse energy, 10 kHz repetition rate SWIR-OPCPA-source, based on a kW-class Yb:YAG pump laser driving a passively CEP stable SWIR seed generation and the subsequent amplification in three broadband degenerate OPA stages. With an output power of up to 49 W this laser setup is currently, to the best of our knowledge, the most powerful few-cycle SWIR OPCPA laser system with stable CEP in terms of average power. The resulting high energy pulses with a center wavelength of 2.1 μm are compressible to below 20 fs. Due to the passively CEP-stable seed pulse generation and an active slow-loop CEP control, the CEP of the pulses can be stabilized with a precision of <100 mrad. Together with the excellent power stability resulting in only 0.8% rms average power fluctuations, our system constitutes a new back-bone of ultrafast science.

2. Layout of the high-power SWIR source

The pump light source we use to drive our self-seeded three stage OPCPA system is an in-house developed Yb:YAG based amplifier chain equivalent to the laser system reported by T. Nubbemeyer et. al. [24]. It consists of an Yb:YAG fiber oscillator, whose pulses are stretched to ns pulse duration in a fiber-Bragg-grating and subsequently amplified in an Yb:YAG fiber-amplifier, a regenerative Yb:YAG thin-disk pre-amplifier and a regenerative Yb:YAG thin-disk power-amplifier. Currently, the main power-amplifier is capable of delivering more than 530 W of average power at 10 kHz repetition rate. The 1030 nm wavelength pulses from this pump source are compressed to 1.2 ps duration in a grating compressor with ~85% throughput efficiency. While being a high-power laser source, the Yb:YAG thin-disk amplifier still exhibits an excellent power stability and beam quality with only 0.3% rms average power fluctuations over multiple hours of operation and an M^2 of 1.1. These properties make the laser a well-suited pump light source for our SWIR OPCPA. The remaining 465 W after compression are used to drive the self-seeded, high pulse energy, high repetition rate SWIR OPCPA setup. To keep pointing and pulse duration instabilities in the output of the main Yb:YAG thin-disk amplifier to a minimum, two active beam pointing stabilization systems are used in front of the grating compressor and the OPA setup, respectively. The actual OPCPA setup can be divided into the seed generation, dispersion control and power-amplification setups (Fig. 2).

The seed generation setup requires only a small fraction of the available pump power to generate the phase-stable 1.7 to 2.5 µm pulses. The pump light is frequency doubled to 515 nm in a second-harmonic-generation (SHG) stage which is divided into two channels. In the first channel, a supercontinuum (SC) is generated by bulk filamentation (SCG in Fig. 2). This SC was mixed with the remainder of the SHG to generate the CEP-stable SWIR pulses via a difference frequency generation (DFG) process as described in sec. 3. This approach for generating a CEP-stable SWIR seed for the OPA setup allows for a very compact footprint by avoiding the necessity to amplify the desired part of the supercontinuum prior to the DFG. The sub-mW SWIR pulses from the DFG are then amplified to measurable power levels in a first noncollinear OPA stage with a noncollinearity angle of 1.5°. To ensure optimum amplification efficiency and compressibility, the amplified pulses from OPA stage 1 are sent into a dispersion control setup consisting of a combination of dispersive material and chirped mirrors. This setup compensates for the third order dispersion accumulated by the SWIR-pulses throughout the amplification stages and introduces enough positive dispersion to get high amplification efficiency while allowing post-amplification compression by dispersion in sapphire or other negative dispersion materials suitable for transmission of ultrashort multi-mJ pulses. Following the dispersion optimization, the SWIR pulses are subsequently amplified to multi-mJ energies in two additional noncollinear

Optics EXPRESS

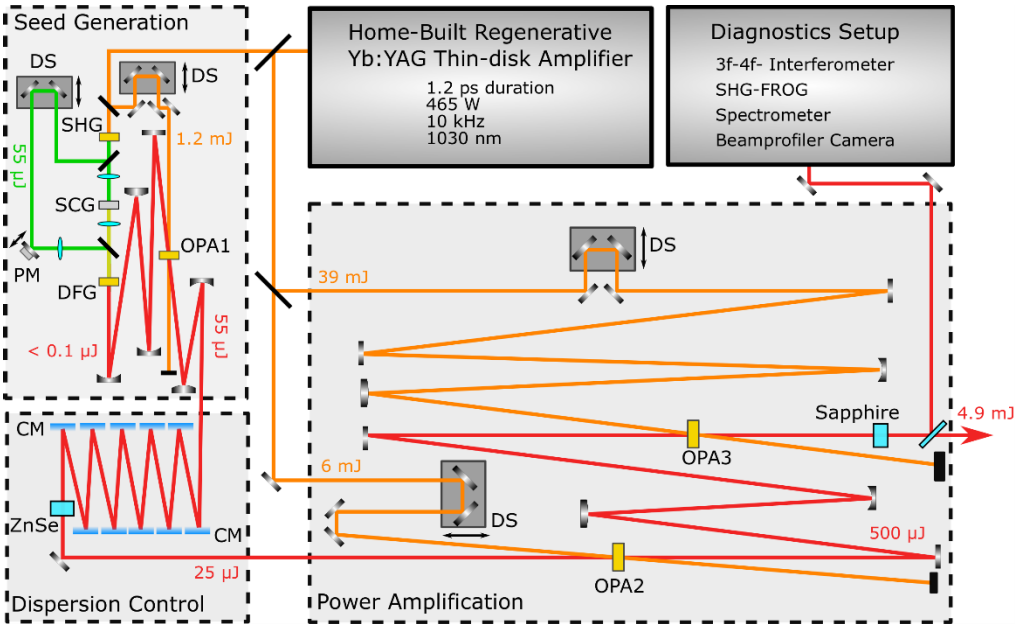

Fig. 2. Schematic drawing of the high power SWIROPCPA setup. CM: chirped mirrors, DFG: difference frequency generation, DS: delay stage, OPA: optical parametric amplification, PM: piezo mirror, SCG: supercontinuum generation, SHG: second harmonic generation.

OPA stages using bismuth triborate (OPA stage 2) and MgO:LiNbO3 (OPA stage 3) crystals. The noncollinearity angles for OPA stage two and three are 2° and 1.9° respectively.

3. CEP-stable SWIR-seed generation

Generating broadband, CEP stable seed pulses is the most crucial part of the OPCPA setup since the bandwidth and noise properties achieved here will limit the performance of the whole laser setup. Thus, a robust and compact design is important to reduce pointing and phase instabilities in the DFG process. We use a thin film polarizer to split off 13 W of average power from the pump beam for the seed generation setup. This 13 W beam is then divided into two beams with 1 W and 12 W of power respectively. The 1-W beam is frequency doubled in a 4-mm BBO crystal, generating 550 mW light at a wavelength of 515 nm (SHG). To generate a signal beam for our DFG process, 15 mW of this SHG are split off by a beam splitter and used to generate a supercontinuum (SC) by bulk filamentation (SCG in Fig. 2). Both YAG and sapphire are possible crystal choices for bulk filamentation using 515 nm picosecond pulses. While sapphire resulted in large spectral bandwidth, the SC generated in YAG had favorable stability regarding pulse energy and spectral shape. Sapphire crystals also require more pulse energy to generate a filament and suffered laser induced damage more frequently. Therefore, we use a 6 mm thick YAG crystal to generate our SC. The spectral components in the range between 650 and 750 nm (see Fig. 3 a)) are then spatially and temporally overlapped with the remaining 530 mW of the SHG. Both beams are focused into a 3 mm lithium triborate crystal to generate SWIR idler pulses covering the spectral range from 1.7 to 2.5 µm (See Fig. 3 b)) via a DFG process. While BBO has a higher nonlinear coefficient [42], it's narrow acceptance bandwidth for the DFG process mixing 515 nm with a 650-750 nm SC, limited the crystal thickness to below 1 mm for the SWIR pulses to cover the full 1700–2500 nm range. Therefore, lithium triborate (LBO), allowing for a

Optics EXPRESS

larger crystal thickness due to its wider phase matching bandwidth, resulted in an overall higher broadband SWIR emission.

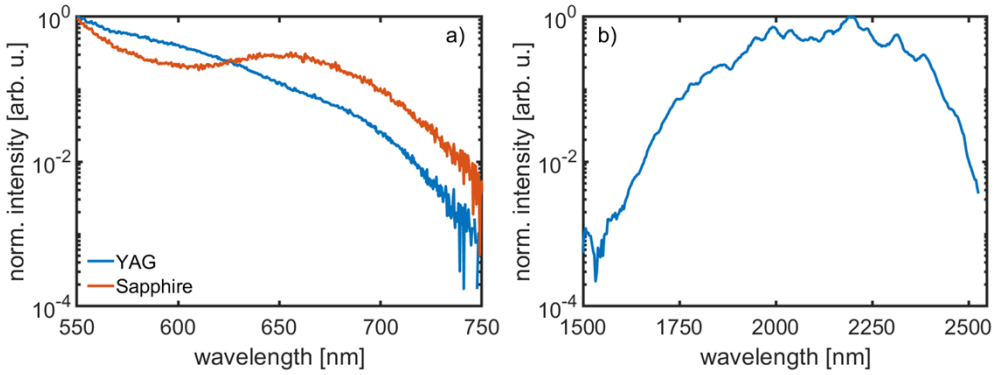

Fig. 3. a) Supercontinuum spectrum generated by bulk filamentation from 15 mW of 515 nm light in a 6 mm YAG crystal. The spectral components below 550 nm have been removed with a spectral filter. b) SWIR spectrum generated in a collinear DFG process mixing 515 nm pump with the 600–750 nm part of the supercontinuum in a 3 mm LBO crystal.

To avoid spatial chirp in the resulting idler pulses, the SC and SHG beams are recombined collinearly using a dichroic mirror in front of the DFG crystal. Following this approach, the resulting small arm length of the interferometer formed by the SC and SHG pump light beam paths helps to reduce instabilities of the generated SWIR light in terms of power as well as CEP caused by pointing fluctuations of the input beam or changes in the optical path lengths for the involved signal (SC) and pump (SHG) beams. The SWIR pulses centered at 2.1 µm wavelength generated in this DFG process are passively CEP stable due to the fact that the SHG- and SC-beams have identical phase noise which then cancels out during the DFG process. In contrast to intrapulse-DFG processes, however, the CEP of the generated pulses is not exactly zero but has a finite but static phase determined by the path length difference of this interferometer. This leads to slow CEP drifts due to path length changes caused by pointing or thermal drifts which are typically occurring on time scales of hours to seconds. These drifts need to be compensated to achieve long-term CEP stability and also present a simple way for active control of the relative CEP value (see sec. 6). In total, we generate a broadband SWIR seed beam with up to 3 mW power from difference frequency mixing in a 3 mm thick LBO crystal, cut in XY-plane for type 1 phase matching with $\vartheta = 90°$, $\varphi = 10.6°$. Optimizing the conditions for stability and bandwidth, however, typically limits the DFG output to just below 1 mW. This power was insufficient for the characterization and optimization of dispersion, beam profile and output power of the pulses. Therefore, we amplify the SWIR idler in a first OPA stage pumped by the remaining 12 W of the 1030 nm fundamental beam that was split off for the seed generation setup. Both, SWIR-seed and fundamental pump beam, are focused into the first OPA crystal to a $1/e^2$-beam diameter of 1.5 mm under a noncollinearity angle of 1.5°.

Multiple types of amplification crystals for 1030-nm-driven 2.1 µm OPAs can be used such as beta-barium borate (BBO), bismuth triborate (BiBO), magnesium oxide doped lithium niobate (LNB), lithium triborate (LBO), potassium titanyle arsenate (KTA) and yttrium calcium oxyborate (YCOB). They all come with different strengths and limitations. As BBO is less costly than BiBO, has a much higher damage threshold than LNB and a larger amplification bandwidth than YCOB or KTA, it is the most suitable crystal for the first OPA stage. With a pump peak intensity of ~100 GW/cm^2, the achievable bandwidth optimized output power from the used 4 mm BBO crystal with a cutting-angle of $\vartheta = 21.4°$ amounts to 550 mW. However, after passing through the dispersion control setup, described in more detail below, only 250 mW are left to seed the

Optics EXPRESS

power-amplification stages. At output powers beyond the few-W regime, OPA stages based on BBO suffer from the residual absorption of spectral components above 2300 nm, resulting in drastic temperature increase and eventual thermally induced damage [43]. This effect prevents the usage of BBO in our power amplification stages.

4. Broadband amplification to multi-mJ energies

As the pulses generated in the seed generation setup do not have sufficient pulse energy for high-cutoff HHG, broadband amplification of the SWIR pulses is necessary. The amplification process has to preserve the spectral bandwidth, CEP stability, and pulse energy stability of the seed pulses and must not introduce distortions in the spatio-temporal profile of the SWIR-beam. Achieving this requires the right choice of amplification crystals, and a careful management of thermal loads and beam sizes throughout the setup to avoid thermal and nonlinear lenses. We observed a nonlinear lens forming in air due to the high peak power of our 1.2 ps 465 W compressed pump beam which can cause damages to mirrors, crystals or even water-cooled beam dumps. Fully avoiding this nonlinear lens caused by propagating through several meters of air would only be possible by operating the laser setup in a vacuum. However, the effect can be mitigated by increasing the beam diameter of the pump light, effectively shifting the focal spot of the nonlinear lens far beyond the actual length of our setup. Therefore, we expand our pump beam from the Yb:YAG TD power-amplifier to a diameter of 15 mm prior to compression in the grating compressor. After splitting off the portion used for the seed generation, we divide the remaining ~450 W of pump light into a 60 W channel for OPA stage 2 and a 390 W channel for OPA stage 3. Only after dividing the power between the channels, the beam diameters are reduced from 15 mm to 3 mm in OPA 2 and 12 mm in OPA 3, resulting in peak pump intensities of ~125 GW/cm^2 and ~50 GW/cm^2 on the respective crystals. Additionally, we operate our OPA stages in a regime where the output power of the OPA stages still depends linearly on the applied pump power, avoiding the back-conversion regime and the associated distortions of the spatio-temporal profile of the SWIR-pulses resulting in significant reduction of HHG efficiency [44,45]. The linear dependence of output power on the applied pump power in the chosen operating regime is illustrated in Fig. 4 b) on the example of the third OPA stage.

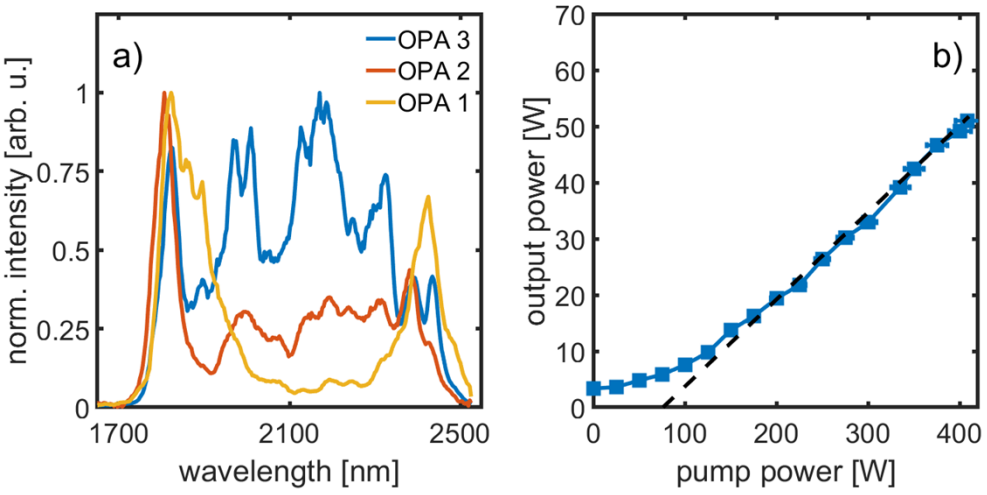

Fig. 4. a) Output Spectra of the three consecutive OPA stages. b) Gain curve of the third OPA stage. The dashed line is a guide to the eye, illustrating the linear relation between pump power and output power. The error bars displayed here are the rms average power fluctuations occurring during a 30 s measurement time for each data point.

Optics EXPRESS

In the second OPA stage we use a 2 mm thick BiBO crystal as BiBO has more favorable absorption properties than BBO and thus suffers less from an increasing temperature due to absorption above 2300 nm [46,47]. The crystal is cut in the XZ-plane with a cutting-angle of $\vartheta = 7.8°$.

A comparison of the input seed spectrum (OPA1) and the output spectrum (OPA2) in Fig. 4 a) shows that the second OPA stage is slightly less broadband and the wavelengths above 2450 nm are not amplified efficiently. We believe this reduction in bandwidth is mainly caused by the rather big noncollinearity angle >2° between the seed and the pump beam, which is necessary to safely split the SWIR from the pump after amplification. The output spectra of the first and second OPA stage both exhibit a distinct spectral shape with peaks in the spectral intensity to both sides of the spectrum and less spectral intensity in the center. This shape is a characteristic feature of the phase matching behavior in degenerate OPA stages when the phase matching angle is slightly detuned from phase matching at the degeneracy frequency. This detuning is introduced to increase the amplification bandwidth of the first two OPA stages at the cost of a slightly reduced amplification gain. Higher amplification bandwidth could be achieved by further detuning the phase matching angle of the crystal, but at a cost of a significant reduction in amplification gain.

In the final OPA stage (OPA 3) the ~390 W of pump power used for amplification impose even more challenging requirements to the nonlinear crystal. The high energy of the pump pulses makes it necessary to significantly increase the beam size in order to avoid peak intensities above the damage threshold of the crystal. Therefore, BiBO can no longer be used at such high powers as BiBO crystals with clear apertures >15 mm are not readily available. KTA and YCOB crystals are available in large sizes and have damage thresholds superior to BBO or BiBO but result in a limited bandwidth of the SWIR output pulses since KTA does not support broadband phase matching in this spectral region and the low nonlinear coefficient of YCOB demands for thicker crystals. LNB has a low damage threshold compared to BBO and BiBO and photorefractive effects can lead to a catastrophic runaway focus process resulting in crystal damage at peak intensities exceeding 50 GW/cm^2 of the pump light [43,48]. Even at a pump power of 390 W, however, large aperture diameter LNB crystals easily allow the beam sizes necessary to keep the peak intensity below the damage threshold. The broadband phase matching conditions and a strong nonlinearity with a nonlinear coefficient of d_{eff}>4 pV/m [42] enable broadband and efficient amplification even at lower pump peak intensities. Additionally, LNB has a low absorption coefficient over the full spectral range of our SWIR pulses [49], resulting in a reduced thermal load as compared to BBO or BiBO crystals. Despite the low absorption coefficient, the crystal temperature rises under full power operation reaching a steady equilibrium temperature of 40°C. The LNB crystals used here are cut at a phase matching angle of $\vartheta = 42.9°$ and are mounted into motorized mirror mounts providing an easy way to compensate the temperature induced shift in optimum phase matching angle by tilting the crystal. Comparing the spectrum of the SWIR pulses after amplification in a 2.2 mm LNB to 49 W of average power in Fig. 4 a) with the spectra recorded for the previous amplification stages shows no further decrease in spectral bandwidth. In contrast to the first and second OPA stage, the output spectrum of OPA stage three shows a higher spectral intensity in the center of the spectrum reflecting the more Gaussian gain profile as detuning the phase matching angle was not necessary due to the large acceptance bandwidth of the LNB crystal. The spectrum of the amplified pulses supports a Fourier-transform-limit (FTL) of 17 fs. Benefiting from the compact setup, excellent stability with below 0.8% rms average power fluctuations for approximately one hour of operation can be achieved (Fig. 5).

The beam quality parameter was investigated at various pump powers for the third OPA stage in the double LNB crystal configuration. The 4-σ beam diameter was determined from images taken with a 17 µm pixel pitch microbolometer camera. At pump powers < 280 W the M^2 value was measured to be ~1.5 in X- and 1.6 in Y-direction. When the pump power was increased beyond this threshold, the beam quality gradually decreased resulting in an M^2 value of ~1.6 in

Optics EXPRESS

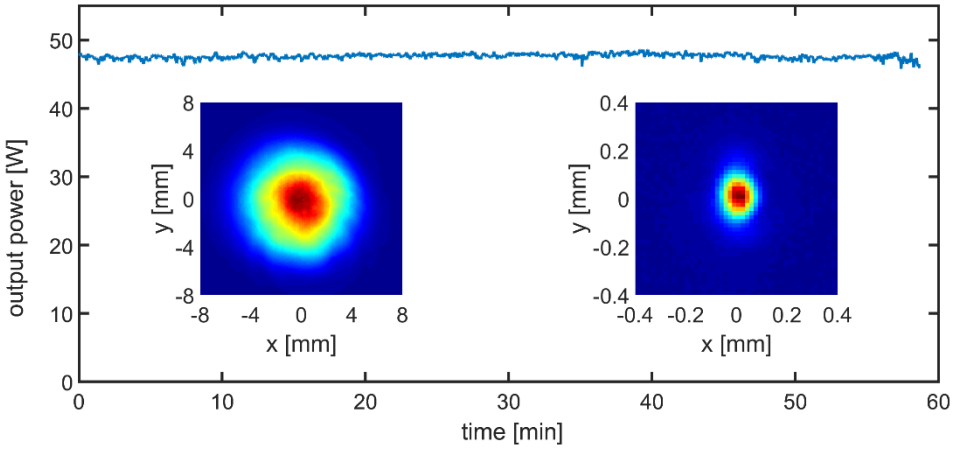

Fig. 5. Output power of the high-power SWIR OPCPA setup measured over 60 min with an average power of 47.6 W and 0.8% rms power fluctuations. The maximum average power achieved was 49 W. The insets show the beam profile of the multi-mJ output pulses with a $1/e^2$ diameter of 14 mm measured with an 80 µm pixel pitch pyroelectric camera (left) and the beam profile in the focus of a 500 mm CaF_2 lens with a $1/e^2$-diameter of 130 µm in X and 190 µm in Y-direction, measured with a 17 µm pixel pitch microbolometer camera (right).

X- and 1.8 in Y-direction at a pump power of 390 W. This decrease in beam quality is likely to be caused by a thermal lensing effect in the two $LiNbO_3$ crystals of the third OPA stage and leads to the development of a non-Gaussian beam profile after the focus. Despite this distortion, the SWIR beam is still focusable with a nearly Gaussian shape in the focus as can be seen in Fig. 5 (inset on the right).

5. Pulse compression and temporal characterization

Since this laser system is meant to drive HHG with cutoff energies well into the water window, it is essential to generate few-cycle pulses, as it increases the available peak intensities and enables the utilization of amplitude gating for isolated attosecond pulse generation. The generated SWIR spectrum after amplification in the three OPA stages shown in Fig. 4(a)) supports a Fourier-limited pulse duration as short as 17 fs, corresponding to 2.4 optical cycles at 2.1 µm center wavelength. We use a combination of Sapphire, ZnSe and custom chirped mirrors to control the dispersion of the SWIR pulses to maximize the amplification efficiency as well as to compress the output pulses of the third OPA stage. The supercontinuum used as a signal during the DFG process generating the CEP-stable seed pulses is chirped due to positive dispersion in the YAG crystal used to generate the SC light. Due to the mixing process in the LBO crystal generating the difference frequency of the overlapping SHG and SC fields, the chirp is reversed for the generated idler. Hence, the resulting SWIR-seed-pulses have negative chirp. Most transparent materials, however, including the amplification crystals used in OPA stage 2 and 3 and the sapphire material meant to compress the pulses later on, introduce negative group-velocity-dispersion (GVD). While materials like ZnSe or multilayer chirped mirrors can be used to induce positive second order dispersion, both of these options are not suitable for compressing high energy, few-cycle pulses due to damage thresholds, thermally induced dispersion shifts and random quasi phase matching [50–52]. Therefore, to ensure good temporal profile matching between the SWIR signal and 1030 nm pump pulses, we implemented a dispersion control setup in between the first and second OPA stage consisting of 10 mm ZnSe and two types of custom chirped mirrors with eight and two bounces, respectively. Due to the large amount of dispersive material in our setup, the third

Optics EXPRESS

order dispersion (TOD) cannot be neglected when trying to compress the pulses close to their FTL. This issue, however, is addressed by the chirped mirrors in the dispersion control setup.

The first set of chirped mirrors was reported in [43] and accumulates negative TOD and positive GDD compensating 40 mm of sapphire during the eight bounces on the mirrors. Together with the positive dispersion of the 10 mm ZnSe we introduce enough GDD to first compensate for the native negative second order dispersion of the SWIR pulses and then stretch the pulses to a duration allowing for high efficiency in the subsequent OPA stages. The remaining TOD of the output pulses is (pre-) compensated by two passes on the second type of chirped mirrors, which introduce negative TOD while having little effect on the second order dispersion of the pulses. Pre-compensating the TOD allows us to compress the pulses after the power amplification to the multi-mJ range, solely by introducing 18 mm sapphire, including entrance windows to our vacuum beamline and pick-off-windows for diagnostics later on. The fine tuning of the pulse duration is done using a pair of fused silica wedges. At a $1/e^2$ beam diameter of 14 mm the estimated B-integral in the compression material amounts to 0.37 rad, which is small enough to not expect a degradation of the beam quality due to nonlinear effects in the solid-state compression unit. We also do not observe a change in spectrum or beam profile of the output pulses when the compression material is inserted, even at a reduced beam diameter of 10 mm.

At OPA 3 an output power of up to 49 W was achieved from a single 2.2 mm thick LNB crystal. The generated SWIR pulses were characterized using a SHG-FROG measurement, yielding a 20.4 fs pulse with 89% of the intensity confined in the main pulse (Fig. 6 b)).

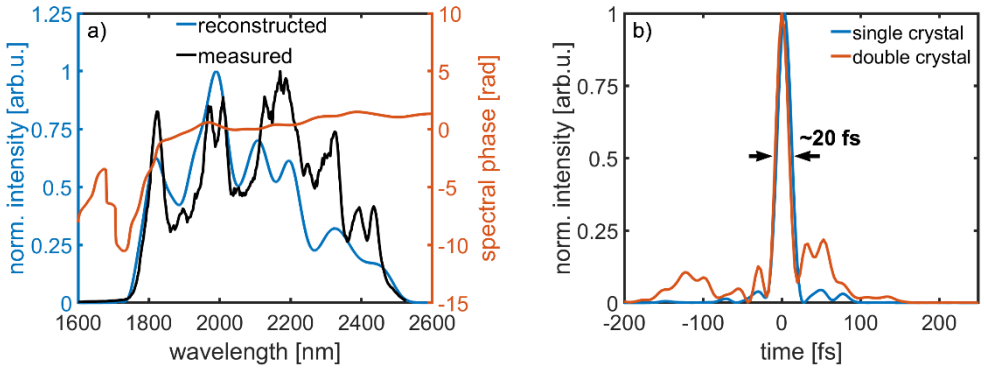

Fig. 6. a) Spectrum of the 49 W SWIR output pulses of the high power OPCPA setup using a singular 2.2 mm LNB crystal (black) as well as the reconstructed spectrum (blue) and spectral phase (red) from a SHG-FROG measurement. b) Reconstructed temporal pulse profiles of the SWIR pulses after amplification in the third OPA stage showing a 20.4 fs pulse duration using a single 2.2 mm LNB (blue) and an 18.5 fs pulse duration using the double crystal approach with two 1.2 mm LNB crystals (red). The double crystal approach results in an increased energy transfer from the main pulse into a pedestal, post- and pre-pulses.

Shorter pulses with 18.5 fs duration were achievable with a double crystal approach using two 1.2 mm LNB crystals phase matching different parts of the input spectrum. This technique is widely used to achieve a higher amplification bandwidth while still having the benefits of a thick crystal [53]. However, the shorter pulse duration was achieved at cost of an average output power reduction to 40 W and the use of two crystals in a noncollinear geometry, led to the development of modulations in the output spectrum which result in either formation of multiple pulses or an energy transfer from the main pulse to a pedestal with a duration of several hundred of fs. To counter this effect, we mounted the two 1.2 mm thick LNB crystals into the same mount to keep the distance between the crystals with ~1 mm as small as possible. This approach achieved the best results despite the fact that the phase matching angle of the two

Optics EXPRESS

crystals cannot be adjusted independently. Additionally, careful alignment of the input beams, a small noncollinearity angle and operating the crystals in a walk-off-compensating scheme [54,55], helped to mitigate those effects, resulting in a decently compressible pulse. The temporal reconstruction of an SHG-FROG measurement is displayed in Fig. 6 b). A compressed pulse duration down to 18.5 fs could be achieved with ~50% of the total pulse energy contained in the main pulse. This suggests, that using a single crystal is preferable when aiming for the highest peak powers, whereas experiments relying on the shortest possible pulses for nonlinear processes such as amplitude gating in HHG could benefit from the double crystal approach. We note here that the 2.6-2.8-cycle duration achieved directly from the OPA output using the double and single crystal approach, respectively, is not short enough to allow for amplitude gating. This can be achieved by an additional nonlinear compression stage based on a hollow-core fiber in the future enabling generation of sub-1.5 cycle pulses.

6. CEP stability

The concept to achieve a highly stable CEP of our output pulses relies on the passively CEP stable seed generation, a CEP preserving amplification and a slow-loop CEP control consisting of a spectral 3f-4f-interferometer to measure the relative CEP and to generate a feedback signal for the piezo mirror (PM in Fig. 2) in the seed generation setup. Typically, f-2f-Interferometers are used to measure the relative CEP fluctuations by recording the spectral interference fringes that form when a pulse is spatio-temporally overlapped with its second harmonic. However, since the bandwidth of our SWIR pulses is not octave spanning such a device would require additional spectral broadening. Thus, we use a 3f-4f-interferometer, observing the spectral fringes of a surface third harmonic (THG) and a 4^{th} harmonic generated by frequency doubling the SWIR-pulses in two subsequent BBO crystals. This approach avoids the additional phase noise introduced by a bulk filamentation nonlinear broadening stage, which is known for strong phase-to-intensity- and phase-to-pointing-noise coupling [56,57]. The relative CEP of our pulses measured by this in-loop 3f-4f-interferometer is used to generate an error signal for the active piezo mirror in the seed generation setup as a phase shift of the pump light relative to the signal directly translates into a shift in the CEP of the SWIR pulses generated in the DFG process [43]. For the characterization of the CEP stability achievable with our laser system, we used a second collinear 3f-4f-interferometer for out-of-loop measurements. Figure 7 shows the relative CEP of the SWIR output measured by the out-of-loop 3f-4f-interferometer. The measurement was taken while driving OPA stage 3 with the full 390 W of pump power in a double LNB crystal configuration. The total rms CEP fluctuations during the ~75 min recording time amount to 92 mrad.

Figure 7 clearly shows that the slow loop CEP control is capable to efficiently suppress slow CEP changes due to interferometric path length changes in the seed generation setup. We note here that we can't achieve single shot detection of the relative CEP due to the limited data acquisition rate of spectrometers used to record the spectral interference fringes encoding the relative CEP. For the data shown in Fig. 7 we were integrating for 20 ms per sample, corresponding to 200 laser shots of our 10 kHz laser, thus limiting us to the detection of fluctuations below 25 Hz. Faster fluctuations however, should not be present due to the passively CEP stable nature of the seed generation. A remaining noise source, causing the rare phase jumps that can be seen in Fig. 7, was identified to be the laser beam pointing stabilization after the compressor for the 1030 nm pump light which was occasionally over compensating and causing a phase shift too fast for our slow-loop-CEP stabilization to follow.

Optics EXPRESS

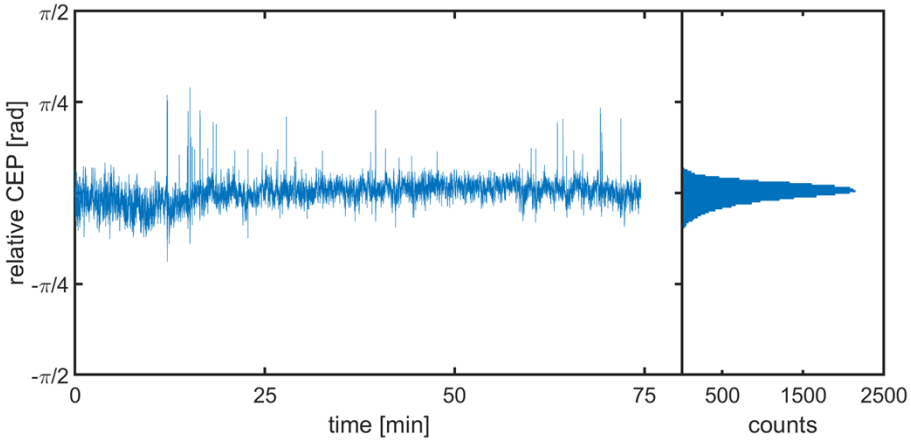

Fig. 7. Relative CEP of the SWIR output at full power after OPA stage 3 measured out-of-loop (left). A histogram of the measured relative CEP values (right).

7. Conclusions

The demonstrated laser system achieves, to the best of our knowledge, the highest average power among few-cycle CEP-stable SWIR-OPA light sources. Its unique combination of 4.9 mJ pulse energy, few-cycle pulse duration and excellent stability with 0.8% average power fluctuations and sub-100 mrad carrier-envelope-phase noise make this setup an ideal choice for advanced attosecond spectroscopy experiments with photon energies well into the soft-X-ray regime.

Further spectral broadening by self-phase modulation in multi-pass cells [58], arrays of thin plates [59] or hollow core fibers [60] and compression close to single-cycle duration has proven to be possible for similar pulses [58–63] and may be implemented for this setup in the future. Scaling the pulse energy beyond the 4.9 mJ of OPA stage 3 is possible, making use of the full 1 kW potential output power of the Yb:YAG pump laser. However, this requires substantial parts of the OPCPA setup to be operated under vacuum conditions to avoid nonlinear lensing in air. Alternatively, the repetition rate of our OPCPA can be increased to achieve higher output power while keeping the pulse energies stable. Operating our OPCPA at up to 20 kHz has already been tested for the seed generation setup. Extending this repetition rate increase to the power amplification stages, however, remains challenging due to the significant increase of thermal load in the setup. The high repetition rate of our multi-mJ OPCPA allows for short measurement times and observation of rare events which would otherwise be hidden by noise.

This OPCPA setup will be used as a frontend for an attosecond beamline combining the attosecond time resolution achievable with HHG sources with photon cutoff energies in the water window thus allowing for experiments and applications in wide range of fields ranging from AMO physics, over chemical and material sciences, to biological applications.

Funding. Chemical Sciences, Geosciences, and Biosciences Division (DE-SC0063); Max-Planck-Gesellschaft (MP Fellow, MPSP); Laserlab-Europe (871124).

Acknowledgments. The authors thank Ferenc Krausz for supporting the project and providing the infrastructure at the MPQ. The authors thank Nicholas Karpowicz and Haochuan Wang for helpful discussions.

Disclosures. The authors declare no conflicts of interest.

Data availability. Data underlying the results presented in this paper are not publicly available at this time but may be obtained from the authors upon reasonable request.

References

Optics EXPRESS

1. M. Hentschel, R. Kienberger, C. Spielmann, G. A. Reider, N. Milosevic, T. Brabec, P. Corkum, U. Heinzmann, M. Drescher, and F. Krausz, "Attosecond metrology," Nature **414**(6863), 509–513 (2001).
2. C. Bressler and M. Chergui, "Ultrafast x-ray absorption spectroscopy," Chem. Rev. **104**(4), 1781–1812 (2004).
3. M. Lucchini, S. A. Sato, G. D. Lucarelli, B. Moio, G. Inzani, R. Borrego-Varillas, F. Frassetto, L. Poletto, H. Hübener, U. De Giovannini, A. Rubio, and M. Nisoli, "Unravelling the intertwined atomic and bulk nature of localised ex-citons by attosecond spectroscopy," Nat. Commun. **12**(1), 1021 (2021).
4. A. Moulet, J. B. Bertrand, T. Klostermann, A. Guggenmos, N. Karpowicz, and E. Goulielmakis, "Soft x-ray excitonics," Science **357**(6356), 1134–1138 (2017).
5. M. Freiwald, S. Cramm, W. Eberhardt, and S. Eisebitt, "Soft x-ray absorption spectroscopy in liquid environments," J. Electron Spectrosc. Relat. Phenom. **137-140**, 413–416 (2004).
6. D. Drevon, M. Görlin, P. Chernev, L. Xi, H. Dau, and K. M. Lange, "Uncovering The Role of Oxygen in Ni-Fe(O_xH_y) Electrocatalysts using In situ Soft X-ray Absorption Spectroscopy during the Oxygen Evolution Reaction," Sci. Rep. **9**(1), 1532 (2019).
7. S.-C. Lin, C.-C. Chang, S.-Y. Chiu, H.-T. Pai, T.-Y. Liao, C.-S. Hsu, W.-H. Chiang, M.-K. Tsai, and H. M. Chen, "Operando time-resolved X-ray absorption spectroscopy reveals the chemical nature enabling highly selective CO_2 reduction," Nat. Commun. **11**(1), 3525 (2020).
8. Z.-H. Loh, G. Doumy, and C. Arnold, *et al.*, "Observation of the fastest chemical processes in the radiolysis of water," Science **367**(6474), 179–182 (2020).
9. D. E. Rivas, S. Serkez, and T. M. Baumann, *et al.*, "High-temporal resolution x-ray spectroscopy with free-electron and optical lasers," Optica **9**(4), 429–430 (2022).
10. J. Miao, R. L. Sandberg, and C. Song, "Coherent x-ray diffraction imaging," IEEE J. Sel. Top. Quantum Electron. **18**(1), 399–410 (2012).
11. F. Remacle and R. D. Levine, "An electronic time scale in chemistry," Proc. Natl. Acad. Sci. U.S.A. **103**(18), 6793–6798 (2006).
12. J. Duris, S. Li, and T. Driver, *et al.*, "Tunable isolated attosecond x-ray pulses with gigawatt peak power from a free-electron laser," Nat. Photonics **14**(1), 30–36 (2020).
13. S. Serkez, G. Geloni, S. Tomin, G. Feng, E. Gryzlova, A. Grum-Grzhimailo, and M. Meyer, "Overview of options for generating high-brightness attosecond x-ray pulses at free-electron lasers and applications at the european XFEL," J. Opt. **20**(2), 024005 (2018).
14. A. Baltûska, T. Udem, M. Uiberacker, M. Hentschel, E. Goulielmakis, C. Gohle, R. Holzwarth, V. S. Yakovlev, A. Scrinzi, T. W. Hänsch, and F. Krausz, "Attosecond control of electronic processes by intense light fields," Nature **421**(6923), 611–615 (2003).
15. T. Popmintchev, M.-C. Chen, and D. Popmintchev, *et al.*, "Bright coherent ultrahigh harmonics in the kev x-ray regime from mid-infrared femtosecond lasers," Science **336**(6086), 1287–1291 (2012).
16. H. Cao, R. S. Nagymihaly, and V. Chvykov, "Cross thin slab kw-class ti: Sapphire amplifiers," Laser Phys. **29**(6), 065802 (2019).
17. V. Chvykov, J. Nees, and K. Krushelnick, "Transverse amplified spontaneous emission: The limiting factor for output energy of ultra-high power lasers," Opt. Commun. **312**, 216–221 (2014).
18. M. Lewenstein, P. Balcou, M. Y. Ivanov, A. L'huillier, and P. B. Corkum, "Theory of high-harmonic generation by low-frequency laser fields," Phys. Rev. A **49**(3), 2117–2132 (1994).
19. J. Tate, T. Auguste, H. G. Muller, P. Salières, P. Agostini, and L. F. DiMauro, "Scaling of wave-packet dynamics in an intense midinfrared field," Phys. Rev. Lett. **98**(1), 013901 (2007).
20. T. Popmintchev, M.-C. Chen, A. Bahabad, M. Gerrity, P. Sidorenko, O. Cohen, I. P. Christov, M. M. Murnane, and H. C. Kapteyn, "Phase matching of high harmonic generation in the soft and hard x-ray regions of the spectrum," Proc. Natl. Acad. Sci. **106**(26), 10516–10521 (2009).
21. Y. Wu, F. Zhou, E. W. Larsen, F. Zhuang, Y. Yin, and Z. Chang, "Generation of few-cycle multi-millijoule 2.5 μm pulses from a single-stage Cr2+: ZnSe amplifier," Sci. Rep. **10**(1), 7775 (2020).
22. I. Moskalev, S. Mirov, M. Mirov, S. Vasilyev, V. Smolski, A. Zakrevskiy, and V. Gapontsev, "140 w cr: Znse laser system," Opt. Express **24**(18), 21090–21104 (2016).
23. Y. Wu, E. Witting Larsen, F. Zhou, L. Wang, A. Marra, D. Schade, J. Li, and Z. Chang, "Transition metal doped zinc selenide infrared lasers for ultrafast and intense field science," in *Emerging Laser Technologies for High-Power and Ultrafast Science*, 2053-2563, pp. 3–1 to 3–23, IOP Publishing, 2021.
24. T. Nubbemeyer, M. Kaumanns, M. Ueffing, M. Gorjan, A. Alismail, H. Fattahi, J. Brons, O. Pronin, H. G. Barros, Z. Major, T. Metzger, D. Sutter, and F. Krausz, "1 kw, 200 mj picosecond thin-disk laser system," Opt. Lett. **42**(7), 1381–1384 (2017).
25. P. Russbueldt, T. Mans, J. Weitenberg, H. Hoffmann, and R. Poprawe, "Compact diode-pumped 1.1 kw Yb: YAG innoslab femtosecond amplifier," Opt. Lett. **35**(24), 4169–4171 (2010).
26. G. Bonati, H. Voelckel, T. Gabler, U. Krause, A. Tünnermann, J. Limpert, A. Liem, T. Schreiber, S. Nolte, and H. Zellmer, "1.53 kw from a single Yb-doped photonic crystal fiber laser," *Photonics West, San Jose, Late Breaking Developments, Session*, vol. 5709, 2005.
27. J. Pouysegur, M. Delaigue, C. Hönninger, Y. Zaouter, P. Georges, F. Druon, and E. Mottay, "Numerical and experimental analysis of non-linear regenerative amplifiers overcoming the gain bandwidth limitation," IEEE J. Sel. Top. Quantum Electron. **21**(1), 212–219 (2015).

Optics EXPRESS

28. M. van Mörbeck-Bock, T. Feng, A. Heilmann, L. Ehrentraut, H. Stiel, M. Hennecke, T. Sidiropoulos, C. von Korff Schmising, S. Eisebitt, and M. Schnürer, "High average power OPCPA MIR-systems for coherent soft x-ray generation accessing absorption edges of metal," Proc. SPIE **11777**, 117770C (2021).
29. M. K. Windeler, K. Mecseki, J. S. Robinson, J. M. Fraser, A. R. Fry, and F. Tavella, "High average power 106 w, 1.75 µm, 100 khz optical parametric chirped pulse amplifier," in *2019 Conference on Lasers and Electro-Optics (CLEO)*, pp. 1–2, IEEE, 2019.
30. T. Feng, A. Heilmann, M. Bock, L. Ehrentraut, T. Witting, H. Yu, H. Stiel, S. Eisebitt, and M. Schnürer, "27 W 2.1 µm OPCPA system for coherent soft X-ray generation operating at 10 kHz," Opt. Express **28**(6), 8724–8733 (2020).
31. T. de Faria Pinto, J. Mathijssen, K. S. E. Eikema, and S. Witte, "Optical parametric chirped pulse amplifier producing ultrashort 10.5 mJ pulses at 1.55 µm," Opt. Express **27**(21), 29829–29837 (2019).
32. Y. Fu, E. J. Takahashi, and K. Midorikawa, "High-energy infrared femtosecond pulses generated by dual-chirped optical parametric amplification," Opt. Lett. **40**(21), 5082–5085 (2015).
33. G. Andriukaitis, T. Balčiūnas, S. Ališauskas, A. Pugžlys, A. Baltuška, T. Popmintchev, M.-C. Chen, M. M. Murnane, and H. C. Kapteyn, "*90 GW peak power few-cycle mid-infrared pulses from an optical parametric amplifier*," Opt. Lett. **36**(15), 2755–2757 (2011).
34. K. Zhao, H. Zhong, P. Yuan, G. Xie, J. Wang, J. Ma, and L. Qian, "Generation of 120 GW mid-infrared pulses from a widely tunable noncollinear optical parametric amplifier," Opt. Lett. **38**(13), 2159–2161 (2013).
35. V. Shumakova, P. Malevich, S. Ališauskas, A. Voronin, A. M. Zheltikov, D. Faccio, D. Kartashov, A. Baltuška, and A. Pugžlys, "Multi-millijoule few-cycle mid-infrared pulses through nonlinear self-compression in bulk," Nat. Commun. **7**(1), 12877 (2016).
36. K.-H. Hong, C.-J. Lai, J. P. Siqueira, P. Krogen, J. Moses, C.-L. Chang, G. J. Stein, L. E. Zapata, and F. X. Kärtner, "Multi-mJ, kHz, 2.1 µm optical parametric chirped-pulse amplifier and high-flux soft x-ray high-harmonic generation," Opt. Lett. **39**(11), 3145–3148 (2014).
37. B. Schmidt, N. Thiré, M. Boivin, A. Laramée, F. Poitras, G. Lebrun, T. Ozaki, H. Ibrahim, and F. Légaré, "Frequency domain optical parametric amplification," Nat. Commun. **5**(1), 3643 (2014).
38. Y. Yin, J. Li, X. Ren, K. Zhao, Y. Wu, E. Cunningham, and Z. Chang, "High-efficiency optical parametric chirped-pulse amplifier in BiB_3O_6 for generation of 3 mJ, two-cycle, carrier-envelope-phase-stable pulses at 1.7 µm," Opt. Lett. **41**(6), 1142–1145 (2016).
39. Y. Deng, A. Schwarz, H. Fattahi, M. Ueffing, X. Gu, M. Ossiander, T. Metzger, V. Pervak, H. Ishizuki, T. Taira, T. Kobayashi, G. Marcus, F. Krausz, R. Kienberger, and N. Karpowicz, "Carrier-envelope-phase-stable, 1.2 mJ, 1.5 cycle laser pulses at 2.1 µm," Opt. Lett. **37**(23), 4973–4975 (2012).
40. J. H. Buss, I. Grguraš, S. Starosielec, M. Petev, T. Golz, M. Schulz, M. Prandolini, P. Kraus, F. Campi, and R. Riedel, "High-power OPCPAs at 1450–2400 nm wavelength," Proc. SPIE **11670**, 116700Y (2021).
41. Y. Fu, K. Nishimura, R. Shao, A. Suda, K. Midorikawa, P. Lan, and E. J. Takahashi, "High efficiency ultrafast water-window harmonic generation for single-shot soft x-ray spectroscopy," Commun. Phys. **3**(1), 92 (2020).
42. S. G. Grechin, "Integral criterion for selecting nonlinear crystals for frequency conversion," Quantum Electron. **39**(2), 171–173 (2009).
43. M. Neuhaus, H. Fuest, M. Seeger, J. Schötz, M. Trubetskov, P. Russbueldt, H. Hoffmann, E. Riedle, Z. Major, V. Pervak, M. F. Kling, and P. Wnuk, "10 w cep-stable few-cycle source at 2 µm with 100 khz repetition rate," Opt. Express **26**(13), 16074–16085 (2018).
44. A. Giree, M. Mero, G. Arisholm, M. J. Vrakking, and F. J. Furch, "Numerical study of spatiotemporal distortions in noncollinear optical parametric chirped-pulse amplifiers," Opt. Express **25**(4), 3104–3121 (2017).
45. C. Jakubeit, "High harmonic generation using a 2 µm OPCPA," PhD thesis, lmu, 2019 (pp. 45–50).
46. G. Bhar, U. Chatterjee, and S. Das, "Tunable near-infrared radiation by difference frequency mixing in beta barium borate crystal," Appl. Phys. Lett. **58**(3), 231–233 (1991).
47. A. Cherepakhin, A. Zaitsev, A. Aleksandrovsky, and A. Zamkov, "Optical and nonlinear optical properties of orthorhombic bib3o6," Opt. Mater. **34**(5), 790–792 (2012).
48. M. Carrascosa, J. Villarroel, J. Carnicero, A. García-Cabañes, and J. Cabrera, "Understanding light intensity thresholds for catastrophic optical damage in linbo 3," Opt. Express **16**(1), 115–120 (2008).
49. P. Sen, P. Sen, R. Bhatt, S. Kar, V. Shukla, and K. Bartwal, "The effect of MgO doping on optical properties of LiNbO3 single crystals," Solid State Commun. **129**(11), 747–752 (2004).
50. G. Gui, A. Adak, M. Dandapat, D. Carlson, D. Morrill, H. Kapteyn, M. Murnane, and C.-T. Liao, "Strong optical nonlinearities in dispersive dielectric chirped mirrors below the damage threshold," in *Laser Science*, pp. JW6A–18, Optica Publishing Group, 2020.
51. H. Krol, C. Grèzes-Besset, L. Gallais, J.-Y. Natoli, and M. Commandré, "Study of laser-induced damage at 2 microns on coated and uncoated ZnSe substrates," in *Laser-Induced Damage in Optical Materials: 2006*, vol. 6403, pp. 382–389, SPIE, 2007.
52. J. Gu, A. Schweinsberg, L. Vanderhoef, M. Tripepi, A. Valenzuela, C. Wolfe, T. R. Ensley, E. Chowdhury, and M. Kolesik, "Random quasi-phase-matching in polycrystalline media and its effects on pulse coherence properties," Opt. Express **29**(5), 7479–7493 (2021).
53. Z. Hong, H. Zhang, and S. Ke, "Efficient Generation of Spectrum-Manipulated Few-Cycle Laser Pulses through Cascaded Dual-Chirped OPA," Int. J. Mol. Sci. **22**(13), 6887 (2021).

Optics EXPRESS

54. A. L. Oien, I. T. McKinnie, P. Jain, N. A. Russell, D. M. Warrington, and L. Gloster, "Efficient, low-threshold collinear and non-collinear beta-barium borate optical parametric oscillators," Opt. Lett. **22**(12), 859–861 (1997).
55. J. Wang, M. H. Dunn, and C. F. Rae, "Polychromatic optical parametric generation by simultaneous phase matching over a large spectral bandwidth," Opt. Lett. **22**(11), 763–765 (1997).
56. A. Baltûska, M. Uiberacker, E. Goulielmakis, R. Kienberger, V. S. Yakovlev, T. Udem, T. W. Hänsch, and F. Krausz, "Phase-controlled amplification of few-cycle laser pulses," IEEE J. Sel. Top. Quantum Electron. **9**(4), 972–989 (2003).
57. B. Maingot, G. Chériaux, N. Forget, and A. Jullien, "Spectral coherence properties of continuum generation in bulk crystals," arXiv, arXiv:2201.01950 (2022).
58. J. Qian, Y. Peng, Y. Li, B. Shao, Z. Liu, W. Li, R. Feng, L. Shen, Y. Leng, and R. Li, "Few-cycle mid-infrared laser based on nonlinear self-compression in solid thin plates," Opt. Lett. **46**(19), 5075–5078 (2021).
59. G. Jargot, N. Daher, L. Lavenu, X. Delen, N. Forget, M. Hanna, and P. Georges, "Self-compression in a multipass cell," Opt. Lett. **43**(22), 5643–5646 (2018).
60. P. Béjot, B. Schmidt, J. Kasparian, J.-P. Wolf, and F. Legaré, "Mechanism of hollow-core-fiber infrared-supercontinuum compression with bulk material," Phys. Rev. A **81**(6), 063828 (2010).
61. V. Cardin, N. Thiré, S. Beaulieu, V. Wanie, F. Légaré, and B. E. Schmidt, "0.42 tw 2-cycle pulses at 1.8 μ m via hollow-core fiber compression," Appl. Phys. Lett. **107**(18), 181101 (2015).
62. P. Wang, Y. Li, W. Li, H. Su, B. Shao, S. Li, C. Wang, D. Wang, R. Zhao, Y. Peng, Y. Leng, R. Li, and Z. Xu, "2.6 mJ /100 Hz CEP-stable near-single-cycle 4μm laser based on OPCPA and hollow-core fiber compression," Opt. Lett. **43**(9), 2197–2200 (2018).
63. T. Nagy, P. Simon, and L. Veisz, "High-energy few-cycle pulses post-compression techniques," Adv. Phys.: X **6**(1), 1845795 (2021).